



Multimodal characterization of carbon electrodes' thermal activation for vanadium redox flow batteries

K. Köble^a, M. Jaugstetter^b, M. Schilling^a, M. Braig^a, T. Diemant^a, K. Tschulik^b, R. Zeis^{a,c,*}

^a Karlsruhe Institute of Technology, Helmholtz Institute Ulm, Helmholtzstraße 11, D-89081, Ulm, Germany

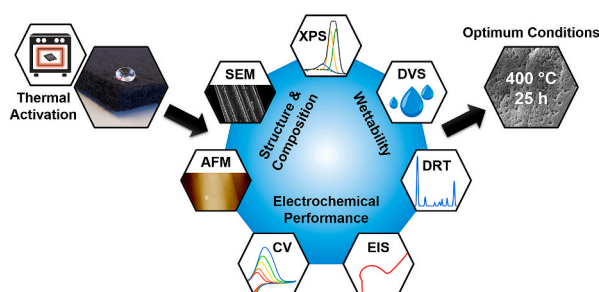
^b Analytical Chemistry II, Faculty of Chemistry and Biochemistry, Ruhr University Bochum, Universitätsstraße 150, D-44801, Bochum, Germany

^c Department of Mechanical and Industrial Engineering, Faculty of Applied Science & Engineering, University of Toronto, 5 King's College Road, Toronto, ON, M5S 3G8, Canada

HIGHLIGHTS

- Carbon felts are characterized by several novel techniques.
- Complementary information on structure, composition, wettability, and performance.
- Probing the wettability of carbon felts employing EIS and DVS.
- Quantifying the wettability of carbon electrodes.
- Determining optimized activation temperature and time.

GRAPHICAL ABSTRACT



ARTICLE INFO

Keywords:

Vanadium redox flow battery
Carbon felt
Atomic force microscopy (AFM)
Dynamic vapor sorption (DVS)
Electrochemical impedance spectroscopy (EIS)
Distribution of relaxation times (DRT)

ABSTRACT

Thermal activation has proven to be a valuable procedure to improve the performance of carbon electrodes in vanadium redox flow batteries (VRFBs). This work investigates how different activation temperatures impact the rayon-based carbon felt's structure, surface composition, wettability, and electrochemical activity. A unique combination of non-standard techniques, including atomic force microscopy (AFM), dynamic vapor sorption (DVS), and electrochemical impedance spectroscopy (EIS) combined with the distribution of relaxation times (DRT) analysis, was used for the first time in the context of VRFB electrodes. The wettability of the carbon felts improved, and the process impedances decreased with higher activation temperatures. However, severe carbon decomposition occurs at high activation temperatures. The optimum electrochemical performance of the carbon felts in the vanadium(IV)/vanadium(V) redox reaction was observed after activation at 400 °C. Thus, we conclude that the optimum activation temperature for this type of carbon felt concerning the investigated properties is around 400 °C. Furthermore, we want to highlight the successful approach of using AFM, DVS, and EIS combined with DRT analysis for an integral investigation of key properties such as structure, wettability, and performance of VRFB electrodes.

* Corresponding author. Karlsruhe Institute of Technology, Helmholtz Institute Ulm, Helmholtzstraße 11, D-89081, Ulm, Germany.

E-mail address: roswitha.zeis@kit.edu (R. Zeis).

1. Introduction

Vanadium redox flow batteries (VRFBs) are a promising technology for large-scale stationary energy storage to accommodate the fluctuating energy output of renewable energy sources [1–3]. They exhibit high round-trip efficiencies, long cycle lives, a relatively low environmental impact, fast response times, and a flexible design, enabling independent power and energy adjustment [3–5]. The electrodes play a key role in the cell efficiency and lifetime of VRFBs [4,6–10] and impact the side reactions during operation [11–13]. Porous electrodes based on carbon fibers, such as carbon felts, papers, or cloths, are typically implemented in VRFBs. In contrast to the simple graphite plates used in the first VRFB, developed in the late 1980s by Skyllas-Kazacos et al. [14], the porous carbon materials exhibit a three-dimensional structure with a high active surface area.

However, the pristine electrode materials are relatively inactive towards the vanadium redox reactions and poorly wettable due to their hydrophobic nature [11,15–23]. Different ways to modify the material were proposed, such as metal deposition, chemical treatments with acids or bases, carbon-based modifications, or plasma treatment [6,7]. Still, the most common pretreatment is a thermal activation procedure, which has been reported to increase the active surface area [17,19–21,24–26], introduce functional surface groups [16–22,24–27], improve the wettability [15,18–21,23], and alter the graphitic structure [8,16,21–23,25]. These property changes of the material often coincide, rendering it challenging to deconvolute their contributions to the performance gains. A few publications [19–21] have already shown how different heat treatment conditions impact the properties of carbon paper electrodes. However, these results cannot be easily transferred to carbon felt electrodes due to the considerable differences in thickness, morphology, and composition. In an early study, Sun et al. [18] evaluated different treatment times and temperatures of carbon felts to conclude that a thermal activation procedure at 400 °C for 30 h optimizes the cell performance. They also showed that this process introduces oxygen-containing functional groups on the material's surface and visually improves the electrode wetting, which was later quantitatively confirmed in a synchrotron imaging study by Bevilacqua et al. [15]. Subsequent studies applied the thermal activation procedure at 400 °C to different carbon felt materials [16,17]. They observed that the type of precursor – rayon or polyacrylonitrile (PAN) – and pretreatment – carbonization or graphitization – significantly impact how the material is affected by the activation procedure, which makes it challenging to develop a universal activation protocol. Other recent systematic studies [22,23] focused on a carbon felt electrode made from a PAN precursor and investigated the morphological, microstructural, and chemical changes during thermal activation. They showed that the amount of carbon vacancies and edges influences the electrochemical performance in the vanadium redox reactions. Furthermore, Lindner et al. [22] showed in their study that different stages could be observed during thermal activation, including pore formation and growth due to oxidation. Most of these characterization studies apply standard techniques such as scanning electron microscopy (SEM), gas adsorption measurements, contact angle measurements, x-ray photoelectron spectroscopy (XPS), and cyclic voltammetry (CV) to investigate the structure, surface area, wettability, surface composition, and electrochemical performance of the carbon electrodes.

Herein, we present a multimodal characterization study combining standard techniques and innovative approaches to characterize carbon felt electrodes. For the first time, atomic force microscopy (AFM), dynamic vapor sorption (DVS), and electrochemical impedance spectroscopy (EIS), in combination with distribution of relaxation times (DRT) analysis, is used to study the impact of thermal activation on VRFB electrodes. We concentrate on a well-known thermal activation procedure to prove that the presented techniques are valuable for VRFB electrode characterization. Therefore, graphitized rayon-based carbon felt electrodes for VRFBs are thermally activated at temperatures

between 200 °C and 500 °C. SEM is used to visualize structural alterations, and quantitative analysis results from AFM will complement the visual impressions with insight into the dimensions of the structural changes. DVS will be applied to quantitatively study how the treatment temperature affects the wettability of the carbon felt samples, and XPS results will help to correlate the property changes to the changes in surface composition. The changes in wettability, surface composition, and structure will be correlated to the electrochemical performance in the vanadium(IV)/vanadium(V) reaction, which is assessed using CV and EIS. Finally, DRT analysis will be used to resolve the individual impedance losses and correlate them to the changes in structure and wettability.

2. Materials and methods

2.1. Materials and treatments

The graphitized, rayon-based carbon felts (SIGRACELL® GFA 6 EA) for this study were supplied by SGL Carbon and have a nominal thickness of 6 mm. The activated materials were thermally treated before the measurements using a standard procedure [16–18]. Pristine carbon felt was placed in a covered crucible and heated in a muffle furnace for 25 h at 400 °C in an ambient air atmosphere without gas flow. Furthermore, in order to study the impact of the activation temperature on the carbon felt properties, other samples were prepared according to the same procedure at activation temperatures of 200 °C, 300 °C, 350 °C, 450 °C, and 500 °C. The heating rate was set to 400 °C h⁻¹ in all cases and the samples were kept at the respective temperature for 25 h. The samples were left in the oven to cool down.

The vanadium(IV) electrolyte used for electrochemical measurements was produced by dissolving 0.1 M VOSO₄ (vanadyl sulfate hydrate, 99.9% metal basis, Thermo Fisher) in 2 M H₂SO₄ (96%, Suprapur®, Merck, diluted with ultrapure water (18.2 MΩcm)).

2.2. Materials characterization

The morphology and structure of the materials were investigated using SEM and AFM. SEM was performed on an LEO 1550 VP (Carl Zeiss AG) equipped with an inlens detector applying an acceleration voltage of 3.00 kV. AFM images of single carbon fibers were acquired on a BioScope Resolve instrument (Bruker Corporation) using a ScanAsyst-Air probe with approximately 2 nm tip radius and 15° broadening. For AFM imaging, brushes of carbon fibers were carefully extracted from the carbon felt sample with a tweezer and placed on a Menzel microscopy glass using carbon paste glue. The images were recorded in Quantitative Nanomechanical Mapping mode, displaying the height sensor output. The software NanoScope Analysis 1.8 (Bruker Corporation) was used for the subsequent line scan analysis, during which a zero correction was applied to set the zero point. The displayed images were further post-processed to remove the fiber bending and increase the visibility of smaller features in the images.

XPS measurements were carried out with a Specs XPS system with a Phoibos 150 energy analyzer. The spectra were recorded using monochromatized Al K α radiation (300 W, 15 kV), a detection angle of 45°, and pass energies of 90 eV and 30 eV for survey and detail measurements, respectively. CasaXPS was employed for the peak fit of the XPS results. Shirley-type backgrounds were applied for all regions. While an asymmetric line shape was inserted for the peak of sp²-C, Gaussian-Lorentzian peak shapes were used for all other features.

DVS measurements were performed on a Q5000 Sorption Analyzer (TA Instruments) to study the wettability of the samples by measuring the weight change at various relative humidity (RH) values. The samples (ca. 10 mg) were dried at 80 °C for 16 h and transferred to the instrument. The measurement protocol included an isothermal step at 60 °C for 300 min to remove remaining residues, followed by sorption and desorption isotherms at 25 °C. These isotherms were performed from 0%

to 90% RH under nitrogen gas flow and a dwell time of 90 min for each RH value (exception: 120 min between 80% and 90% RH) to reach an equilibrium after each sorption/desorption step. Applying a ramp of $0.5\% \text{min}^{-1}$, the RH was increased and decreased stepwise in 5% intervals.

2.3. Electrochemical characterization

To study the impact of the changes in structure and wettability on the electrochemical performance of the carbon felt electrodes, CV and EIS were performed in a previously described three-electrode setup with a flow cell [28], developed in-house, and an SP-300 potentiostat (BioLogic Science Instruments). Square pieces ($1.0 \text{ cm} \times 1.0 \text{ cm}$) of the carbon felt samples were used as the working electrode (WE) and electrically contacted by a gold foil (0.25 mm, 99.9975+%, Alfa Aesar). The electrolyte was pressed into the electrode with a syringe before the cell assembly for the hydrophobic samples to ensure sufficient wetting. Compression of 37% was used for all samples. A $2.5 \text{ cm} \times 2.5 \text{ cm}$ piece of carbon felt (SIGRACELL® GFA 6 EA, SGL Carbon) or three stacked $2.5 \text{ cm} \times 2.5 \text{ cm}$ pieces of carbon paper (SIGRACET® GDL 39 AA, SGL Carbon) served as the counter electrode (CE) for CV or EIS, respectively. The different CEs were used to adapt the setup to the necessities of the different electrochemical measurements. CV measurements required a CE with a larger surface area to accommodate higher currents, while a flat electrode was preferential for defined flow conditions during EIS measurements. The CEs were activated at $400 \text{ }^\circ\text{C}$ and electrically contacted by a titanium foil (1.0 mm, 99.2%, Alfa Aesar). An in-house developed hydrogen reference electrode was applied as the reference electrode (RE). Gold wires (\varnothing 0.5 mm, 99.9975+%, Alfa Aesar) were used for the electrical connection between the metal foils and the clamps of the potentiostat. All electrochemical measurements were performed at room temperature in vanadium(IV) electrolyte. Using a peristaltic pump (Masterflex L/S®, Cole-Parmer), the electrolyte was pumped from an electrolyte reservoir through the cell and back to the reservoir in a continuous cycle. Thereby, it first passed the RE followed by the WE and the CE.

CV measurements were performed without flow at several scan rates between 2 mVs^{-1} and 10 mVs^{-1} in different potential ranges from 0.00 V vs. RHE to 1.60 V vs. RHE to cover the region of the vanadium(IV)/vanadium(V) redox reaction. Due to significant differences in peak separation, the potential range was adapted for each sample to cover the reaction's oxidation and reduction peak completely. Each CV measurement was performed with a fresh sample to rule out changes from previous measurements.

A subsequent EIS measurement was performed directly after the CV measurement. During the EIS measurements, the electrolyte was pumped with a flow rate of 15 mLmin^{-1} to ensure steady-state conditions. The measurements were performed in the potentiostatic mode at a potential of 1.05 V vs. RHE, corresponding to the onset of the vanadium (IV) oxidation reaction. A single sinusoidal excitation of 5 mV was applied as the perturbation, and frequencies between 100 kHz and 3.5 MHz were investigated. The EIS data were further analyzed with a MATLAB-based DRT tool [29]. The spectra were fitted with a Gaussian function for the discretization and a regularization parameter of $1\text{E-}9$.

3. Results and discussion

The experimental results presented herein are separated into three sections. The first two sections analyze the effect of thermal activation at different temperatures on the structure, surface composition and wettability of the carbon felt. The final section will deal with the consequential impact on the electrochemical performance in the vanadium(IV)/vanadium(V) redox reaction.

3.1. Structural analysis

The structure and morphology of pristine and thermally activated

carbon felts were investigated using AFM and SEM. This study uses AFM for the first time in the context of VRFB electrodes. Combining qualitative impressions from SEM images and quantitative line scan analysis from AFM images provides valuable insights into the structural changes caused by the thermal activation of carbon felt electrodes. In addition to the lateral dimensions, the depth of rods or pores can be studied. At first glance, the investigated carbon felt material is inhomogeneous and displays local differences in structure and morphology, as previously observed by Rabbow et al. [30,31] for a PAN-based carbon felt. Therefore, different sites of each sample were checked during AFM and SEM imaging, and representative individual carbon fibers were chosen for each presented image.

Fig. 1 displays SEM images of the pristine carbon felt at different magnifications and a detailed look at a single carbon fiber extracted from this sample. These images show that carbon felt is an inhomogeneous material with kinks and edges, reacting differently to various treatment procedures. In general, the carbon felt fibers are disarranged and partially entangled. Furthermore, broken and bent fibers are observed, which can be ascribed to the manufacturing process of the electrodes. In agreement with previous publications [16,17,24], higher magnifications reveal that each rayon-based carbon fiber consists of several bundled rods in contrast to PAN-based carbon felts, which consist of smooth individual fibers [16,17,22,24,26]. Furthermore, the images display spherical impurities in this pristine sample, probably stemming from the manufacturing procedure. Apart from the roundish impurity particles, the surface of the pristine material is relatively smooth and free of pores.

AFM was used to get a more detailed impression of the carbon fibers and quantitatively investigate the fiber structure via line scan analysis. In the context of VRFBs, AFM has thus far only been used to study novel membranes [32–34], interfacial processes [35], or very thin electrodes [36–38]. Due to the difficulties in studying whole carbon felts, which were also experienced by other groups [39], we used a tweezer to extract brushes of carbon fibers from the carbon felt sample for the AFM analysis. Previous reports show that studying individual carbon fibers via AFM is possible and gives valuable insights into their surface morphology and nano-sized features [40–45]. Fig. 1 (d) and (e) display an AFM image and the corresponding line scan across the individual rods of the fiber. In agreement with the SEM images, the AFM image shows the individual rods with a mostly smooth surface and some spherical-shaped impurities. The line scan allows for estimating the rod diameter, which amounts to around $2.6 \mu\text{m}$ as highlighted in Fig. 1 (e). Furthermore, the line scan curve is smooth overall and only displays a few noisy parts due to a slightly rougher surface of the rod on the right side. However, it should be considered that the AFM image might be blurred out due to the strong ascending and descending of the tip on the other parts of the fiber.

Since the pristine carbon felt electrode has a low wettability and electrochemical activity [15–22], a pretreatment procedure is needed to improve its performance for VRFB applications. Here, we first activated the carbon felt using a previously described thermal treatment procedure at $400 \text{ }^\circ\text{C}$ for 25 h [16]. The structural changes caused by this procedure are depicted in Fig. 2. The overall felt structure with the disordered fiber arrangement remained similar and is not presented. A closer look at a single fiber shows that the fiber structure stays intact, and the bundled rods prevail. However, the surface of the individual rods is roughened and displays pores of several nanometers. Similar observations were made for the same material by Dixon et al. [24] In this context, we would like to mention that the SEM and AFM images in Fig. 2 only show one representative fiber, but the degree of roughening varied within the material (Supporting Information, Figure S. 1). Throughout the experiments for this study, we also observed significant differences in roughening of the fibers from different batches (Supporting Information, Figures S. 2(a) and (b)), which was previously reported by Rabbow et al. [30,31] as well for a PAN-based carbon felt. In the previously used batch, we also observed inhomogeneous activation

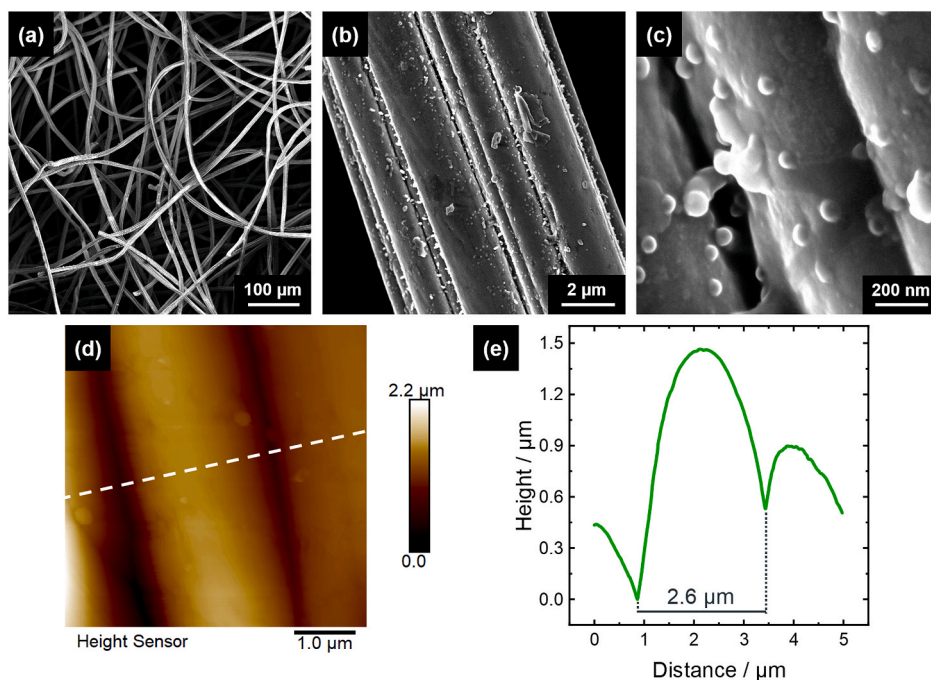


Fig. 1. Top-down SEM images of a pristine SIGRACELL® GFA 6 EA electrode at magnifications of (a) 100x, (b) 5000x, and (c) 50000x. (d) AFM image of an individual fiber extracted from the electrode and (e) corresponding line scan.

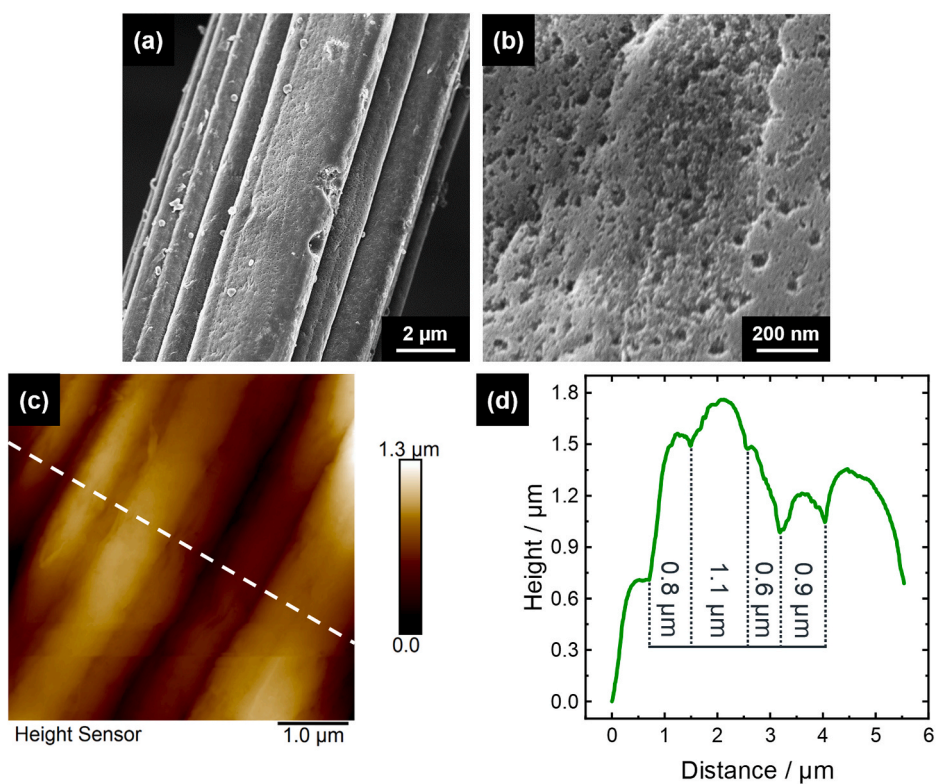


Fig. 2. Top-down SEM images of a SIGRACELL® GFA 6 EA electrode activated at 400 °C for 25 h at magnifications of (a) 5000x and (b) 50000x. (c) AFM image of an individual fiber extracted from the electrode and (d) corresponding line scan.

of the material since fibers extracted from the inside and the outside of the carbon felt showed significantly differing degrees of pore formation and roughening (Supporting Information, Figures S. 2 (b) and (c)).

The AFM image of an individual fiber activated at 400 °C, and the corresponding line scan across the fiber are displayed in Fig. 2 (c) and

(d), respectively. In this case, the individual rods appear significantly thinner than the rods of the pristine sample, and the fiber diameters determined from the line scan analysis range from 0.6 μm to 1.1 μm. However, this is not solely an effect of the thermal treatment; thinner fibers can also be observed in the pristine sample. Depending on which

fiber was chosen and how it was placed on the AFM mount, more or fewer rods are visible from the top view. The AFM line scan across the fiber is noisier than that of the pristine sample indicating a rougher surface of the individual rods. This observation is supported by Fig. 3, which displays AFM images zoomed in on individual rods and the corresponding line scans. These high-resolution images provide insights into the fiber surface morphology and the pores' lateral sizes and depths and can be helpful for an in-depth quantitative analysis of the morphological changes caused by thermal treatment. Fig. 3 (a) and (b) were recorded at similar magnifications, revealing the differences between the pristine and the thermally activated samples. The line scans were performed along an individual rod to investigate the rod surface in contrast to a scan across a whole fiber. The scale of the height profiles of the pristine and the thermally activated sample varies significantly, displaying an overall height change of 73 nm and 198 nm, respectively. This observation implies that the differences in the surface morphology are much more pronounced in the activated sample, which can be ascribed to the observed pore formation and increased roughness. Furthermore, the AFM line scan of the activated sample displays two significant drops in the height of around 98 nm and 49 nm at a distance of around 0.7 μm and 3.1 μm , respectively. The corresponding AFM image shows these drops as pores and rough parts. Similar observations on pore formation in another type of activation procedure were made by Wang et al. [44]. Overall, both line scans display some noise in the nanometer range, which can be attributed to the roughness of the fiber surface itself at these magnifications. Fig. 3 (c) displays a further zoom-in on a single rod of the thermally activated sample, revealing more minor surface features on the individual rod. The line scan across the image provides additional information about the pores' lateral sizes and depths. A small pore can be observed at a distance of around 202 nm with a height drop of 12 nm and a width of 36 nm. A 67 nm wide pore with a height of around 25 nm is visible at a distance of 465 nm. The substantial decrease in height at high distances in the line scan curve can be ascribed to the deepening between the imaged rod and the adjacent carbon fiber rod.

Figs. 1–3 show how a standard thermal activation procedure at

400 °C for 25 h changes the structure and morphology of carbon fibers in a carbon felt sample. The increased roughness and pore formation are consistent with increased surface areas previously observed by several groups [17,19–21,24–26]. The SEM images provide a detailed view of the total carbon felt sample and the individual fibers and rods at different magnifications. AFM is a powerful characterization technique for investigating changes during carbon fiber surface treatments [40–43]. Besides visual impressions of the fiber morphology, it also allows for quantitative analysis of the images using line scans providing information on the size, depth, and shape of pores formed during the activation procedure.

Additional samples were thermally treated at temperatures between 200 °C and 500 °C. The upper limit of 500 °C was chosen since higher temperatures led to complete combustion of the carbon felt. The activation at 200 °C showed no changes in the structure of the carbon fibers. Thus, lower activation temperatures were considered unnecessary for the evaluation. The treatment duration also significantly influences the carbon felts and was previously discussed in other publications [18,19,22,23]. Herein, we chose to focus on the treatment temperature as an example of this multimodal characterization approach. However, the combination of the presented methods benefits an in-depth study on the effect of treatment duration in the future.

Fig. 4 displays SEM images of carbon fibers after activation at different temperatures. Additional activation temperatures were also evaluated via SEM, and the resulting images can be found in the Supporting Information (Figure S. 3). The carbon fiber activated at 200 °C displays the previously described structure with several bundled rods and a few impurities, and the surface of the individual rods is smooth and pore-free, similar to the pristine sample. 350 °C was the lowest activation temperature, at which a change in the morphology could be observed. Fig. 4 (b) shows that the rod surface is rougher than the pristine sample and includes a few pores, but the overall fiber structure remains intact and round-shaped impurities are still visible. 500 °C is the upper-temperature limit used for the thermal activation of carbon felts or carbon paper, typically treated between 400 °C and 500 °C [16–22]. Fig. 4 (c) shows that high temperatures significantly impact the carbon

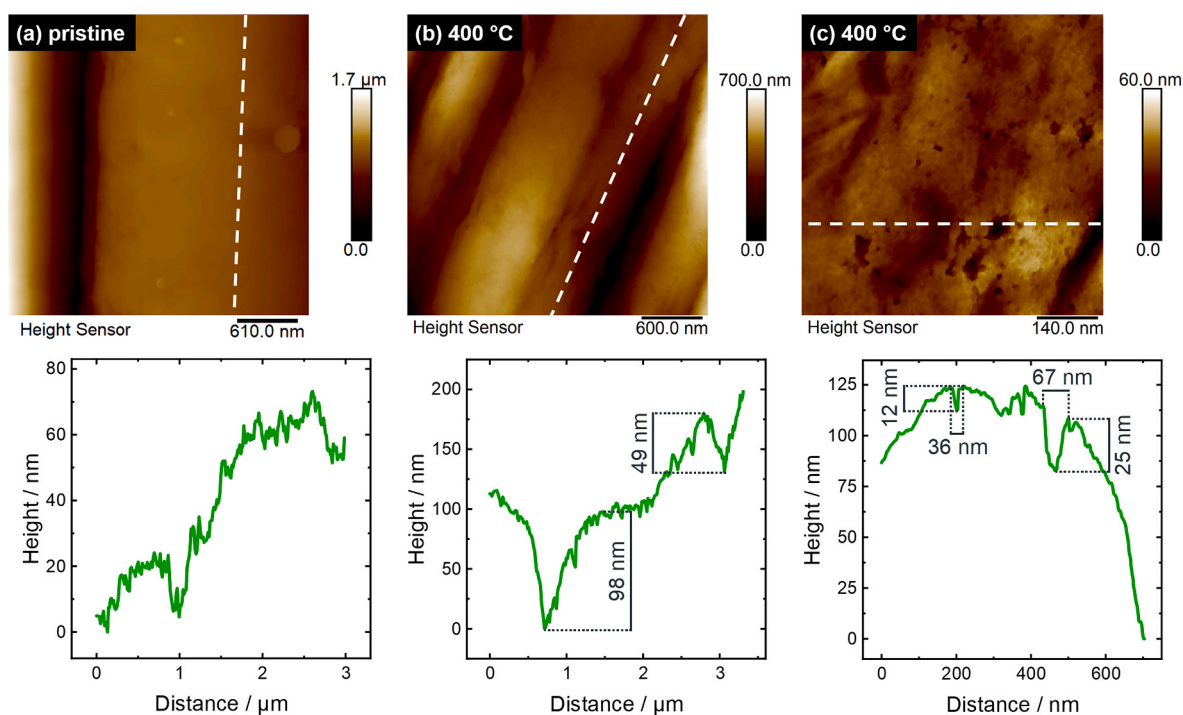


Fig. 3. AFM images (top row) and corresponding line scans (bottom row) of (a) a pristine fiber and (b), (c) a thermally activated fiber (400 °C, 25 h) of a SIGRACELL® GFA 6 EA electrode at different magnifications.

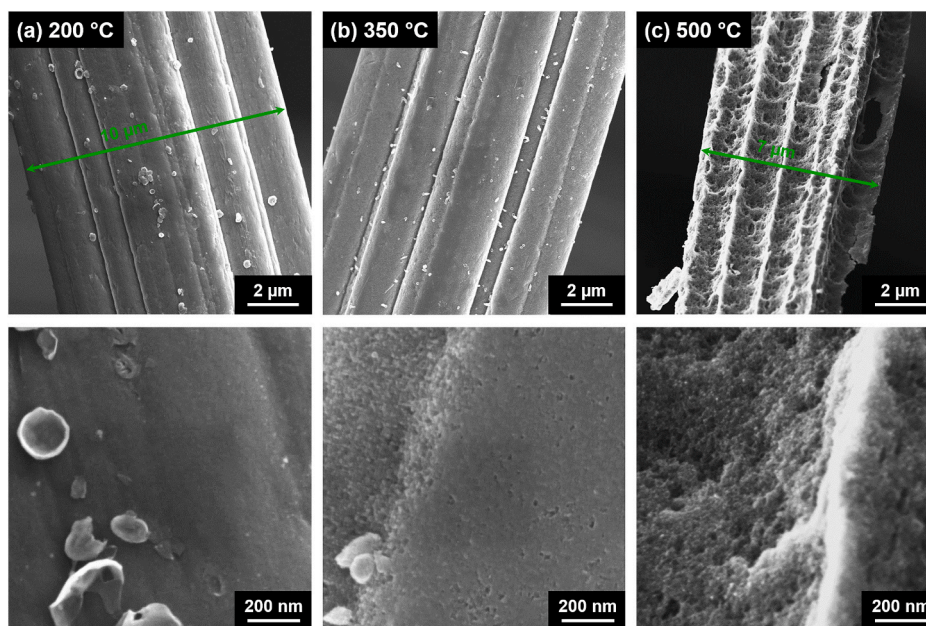


Fig. 4. Top-down SEM images of a SIGRACELL® GFA 6 EA electrode activated at (a) 200 °C, (b) 350 °C, and (c) 500 °C for 25 h at magnifications of 5000x (top row) and 50000x (bottom row).

fiber morphology and surface composition, which will be shown in the following chapter. Overall, the fiber is much thinner after heating at 500 °C, with a width of around 7 μm compared to fiber widths of around 10 μm in the pristine sample. Furthermore, some rods were removed, leading to hollow channel-like shapes. Some parts of the material are barely attached to the fiber (bottom left), and the rod on the right side of the image is severely destroyed, displaying holes and broken edges. The zoom-in on the hollow areas of the fiber reveals a significantly roughened surface without any impurities.

This overview of different activation temperatures shows that activation at lower temperatures, such as 200 °C, does not change the carbon felt morphology, whereas an excessively high temperature, such as 500 °C, destroys the sample. For additional input on the thermal stability of the carbon felt, the weight loss was determined by weighing the samples before and after the thermal treatment and by performing TGA measurements. The results from weighing are depicted in Fig. 5. The samples' weights remain almost constant at low temperatures, with only

about 0.8 wt% weight change at 400 °C. In contrast, 6.2 wt% and 20.5 wt% of the sample weights are lost during activation at 450 °C and 500 °C, respectively. No carbon felt was left after thermal treatment at 600 °C. Due to the air atmosphere during activation, the carbon will be oxidized, and additional oxygen-containing functional groups are formed on the surface, as revealed by the XPS measurements presented in the following section and corroborated by several previous XPS studies [17,18,20–22,24–27]. At higher temperatures, the carbon material decomposes and forms gaseous carbon oxide products [18,20,46], consistent with the observed mass loss. Greco et al. [21] also observed that the surface area increases up to a specific activation time for carbon paper electrodes due to pore formation but decreases beyond that point again. There, the loss of binder material caused the paper to disintegrate. The weight of the carbon felt samples is nearly stable up to 400 °C, implying that the surface is oxidized but not decomposed, and decreases significantly above this temperature due to structural degradation.

Additional results from temperature-ramped TGA measurements are presented in the Supporting Information (Figure S. 4 (a)). They show that significant mass loss is observed above 600 °C and the sample is burned at around 770 °C. However, they can only hint about the thermal stability but do not reflect the conditions during thermal treatment due to the short measurement duration of around 2 h and the constant gas exchange from the applied gas flow. The sample is kept at an elevated temperature for much longer during thermal activation, which explains the delayed mass loss at higher temperatures during the TGA measurement. Furthermore, an exemplary isothermal TGA measurement (see Supporting Information, Figure S. 4 (b)), which mimicked the conditions during thermal activation at 500 °C, showed that higher mass loss is observed during this measurement compared to activation in the muffle furnace. This is due to the constant gas exchange of the gas flow and the smaller amount of sample, which causes a higher surface-to-bulk ratio that can be oxidized more easily.

In conclusion, this section showed that a combination of SEM and AFM images provides significant insights into structural changes of carbon felts and fibers. It revealed that a thermal activation procedure significantly impacts the structure of carbon felts and the morphology of the individual fibers. Low temperatures have little to no effect on the carbon felt, whereas temperatures of 350 °C and 400 °C roughen the surface of the individual rods and oxidize the surface but do not cause

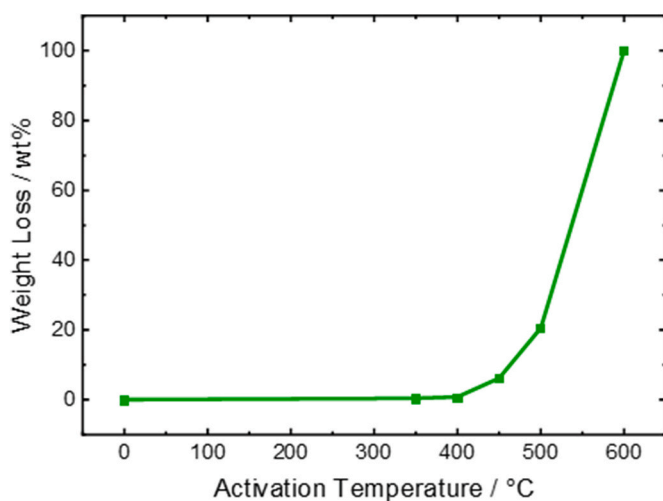


Fig. 5. Relative weight loss during thermal activation as a function of the activation temperature. The weight loss was determined by weighing the carbon felt sample before and after the thermal treatment.

excessive mass loss. Thereby, the surface area increases due to the roughening and the formation of mainly nanometer-sized pores. Furthermore, the overall carbon felt structure remains intact, and the sample can be handled easily. At activation temperatures above 400 °C, the carbon felt is (partially) decomposed and becomes brittle. Both effects are undesirable for an electrode, which must be integrated into a cell setup and withstand the electrolyte flow. The novel approach of using AFM for VRFB electrodes was successfully performed at ambient conditions. It helped to analyze the morphology changes by providing information on the rods' sizes, depths, and shapes and the pores formed during thermal activation. These results can provide a more profound understanding of the morphological changes and quantitative measures of pore formation. Furthermore, AFM can be performed at ambient conditions and offers other measuring modes, which can be used in the future for locally resolved analysis of, e.g., the adhesion.

3.2. Analysis of surface composition and wettability

Besides the structural integrity, the composition and the wettability also play significant roles in the functionality of carbon felt electrodes in VRFBs, and both of these properties go hand in hand. XPS measurements were performed to study the changes in surface composition caused by the thermal treatment procedure. The survey scans of all samples and exemplary peak fits of the C1s and O1s detail scans can be found in the Supporting Information (see Figure S. 5). Fig. 6 (a) and (b) display the analysis of the elemental composition and selected percentages of specific species, which can give an idea of the functional groups in the respective samples. In brief, Fig. 6 (a) shows that there are a maximum of four species above the detection limit, including carbon (C), oxygen (O), sodium (Na), and sulfur (S). The amount of sodium and sulfur is relatively low in all samples and can be ascribed to impurities from the manufacturing process. These two elements have no clear trend, but the amount of impurities generally decreases with higher activation temperatures. Contrarily, the oxygen content increases strongly between the pristine sample (3%) and the sample treated at 500 °C (10%). This observation agrees with previous publications [18,20–22,24,25], which also observed an increased amount of oxygen after thermal treatments. This can be explained by forming of oxygen functional groups due to the oxidation of the carbon felt. Fig. 6 (b) shows that the amount of both types of oxygen functional groups, O=C and O–C, increases with thermal activation temperature. However, no clear trend can be observed which functional group is more favored, which was also previously observed by Greco et al. [20,21] for carbon paper electrodes. In our case, the calculated O=C/O–C ratio (from O1s peak fit) is slightly above 1.0 for all samples. Thus, a slightly higher amount of C=O species is present. The carbon species display different trends. Generally, the amount of carbon species remains relatively stable up to 400 °C and varies only slightly in a range from 94% to 96%. In contrast, after treatment at 450 °C and 500 °C the carbon content decreases to 91% and 90%, respectively. This correlates well to the observed mass loss in the previous section. Higher activation temperatures oxidize the carbon and lead to sample degradation. Consequently, the O/C ratio increases slightly at higher temperatures. The sp³-C (C–C, C–H) amount follows a distinctive trend and decreases from around 21% for the pristine sample to around 8% at an activation temperature of 500 °C. The sp²-C (C=C) reaches a maximum of 69% at 300 °C and decreases again at higher activation temperatures. Lindner et al. [22] observed a similar variation of the sp² carbon content for different treatment durations. The sp³ carbon bonds are preferably oxidized to oxygen functional groups, explaining the reduced amount of C–C and C–H bonds and the higher amount of C=O and C–O bonds. Taken together, the XPS measurements showed a general trend of higher oxygen content at higher activation temperatures. However, there is no clear indication of which species is preferably formed.

The wettability of carbon samples is often influenced by its composition and is a crucial property for VRFBs. A sufficient wettability of the

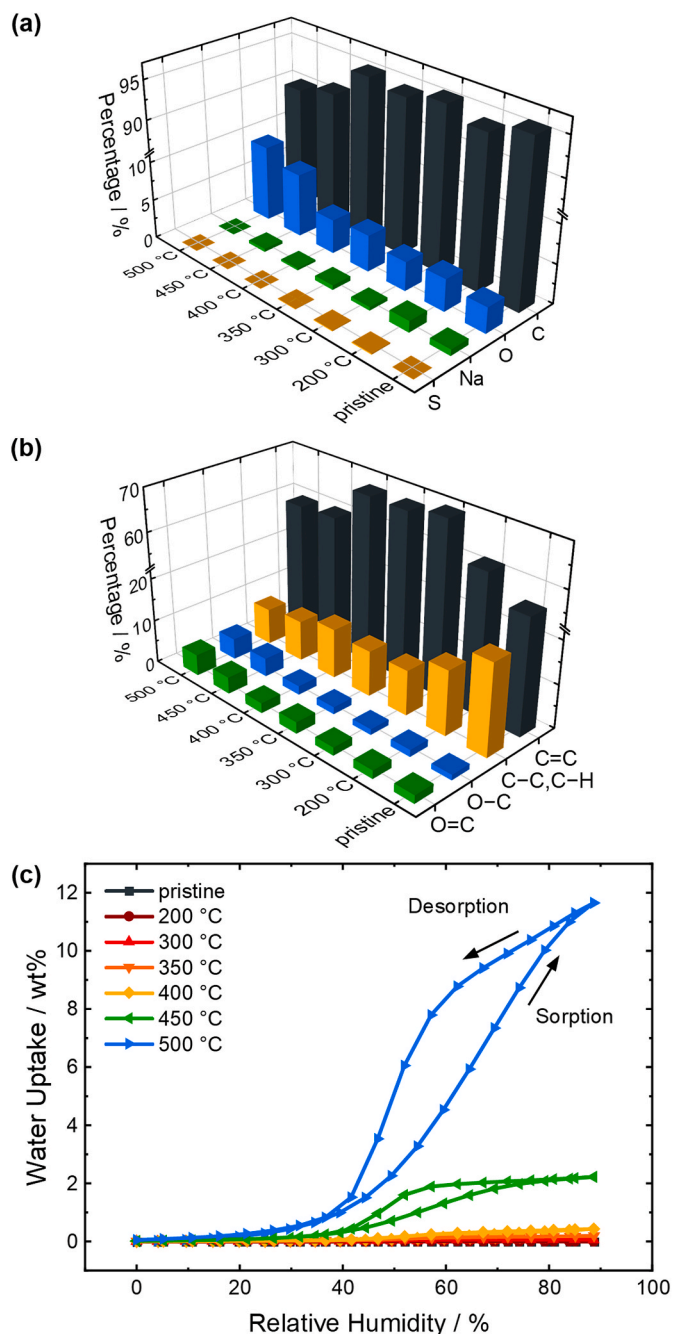


Fig. 6. Analysis of the XPS measurements of pristine and thermally activated SIGRACELL® GFA 6 EA carbon felts, displaying (a) the elemental composition and (b) selected percentages of specific species as a function of treatment temperature. (c) Water vapor sorption and desorption isotherms of the same samples measured at 25 °C.

material is needed since VRFBs are operated with an aqueous electrolyte continuously pumped through the electrode. Higher electrode wettability improves the electrolyte distribution inside the carbon felt and increases the electrolyte-electrode interface, consequently increasing the number of reaction sites, preventing electrode corrosion due to inhomogeneous potential distribution, and improving cell efficiency. Furthermore, improved wettability reduces the pumping losses since the electrolyte is transported more easily through the electrodes.

The wettability of VRFB electrodes is typically investigated using contact angle measurements, which have already been performed by different research groups [20,21,47–49]. The pristine carbon felts are

very hydrophobic, and the contact angles of a water droplet can be measured easily. However, thermally activated samples are typically more hydrophilic and easily absorb a water droplet. This effect renders measurements of the contact angle impossible. The heterogeneity of the carbon felt surface presents another major challenge for this method. Alternative approaches to evaluate the wettability are studying the spreading dynamics [20] or determining the electrode saturation from synchrotron X-ray tomography/radiography [15,49–52]. However, the first approach lacks quantitative information, and the second requires access to a synchrotron facility. Thus, a different approach, which can be performed in-house and delivers quantitative results, is required to compare the significant differences in the wettability of these samples.

Herein, we introduce DVS as an alternative way to study the wettability of carbon felt electrodes. To the best of our knowledge, DVS has so far only been used in the context of redox flow batteries to study membranes [53,54] and mesoporous N-doped carbon spheres [9], but not for the characterization of whole carbon-based electrodes. However, DVS is a powerful tool to investigate natural materials [55–58], such as bamboo, cellulose, or wood, and has also been applied in the research of activated carbons [59–62] and polymer electrolyte membrane fuel cells [63]. Further, compared to synchrotron facilities, this technique combines easy access with the possibility of obtaining quantitative information on the wettability of very different types of materials.

Fig. 6 (c) shows the sorption and desorption isotherms determined from DVS measurements of the different carbon felt samples (Supporting Information, Figure S. 6). Generally, the water uptake increases with the activation temperature applied during the thermal treatment. The pristine sample does not adsorb any water and therefore exhibits no considerable weight change during the DVS measurement. This observation agrees with the contact angle measurements showing hydrophobic contact angles of around 140° [47,49]. The wettability is significantly increased at the standard activation temperature of 400°C , and a maximum water uptake of 0.4 wt% was measured at 90% RH. However, higher activation temperatures such as 450°C and 500°C further improve the wettability, increasing the water uptake to 2.2 wt% and 11.7 wt% at 90% RH, respectively. The increased surface roughness causes increased water uptake and surface area of the activated carbon felts. Furthermore, there seems to be a correlation between the surface composition and the wettability since a higher amount of oxygen functional groups on the surface, found during XPS measurements, improves the water vapor sorption capacity. The sigmoidal shape of the sorption curve remains similar at different activation temperatures and is characteristic of the type V sorption isotherm [64,65]. For all samples with significant wettability, the water uptake only increases slightly up to around 30% RH due to the weak vapor-adsorbent interactions.

In contrast to the sorption behavior of other natural carbon-based materials [55,57,58], no monolayer is formed on the sample surface, and only the favorable polar sites, such as the surface oxides, interact with the water vapor [62–65]. At higher RHs, an exponential increase in water uptake is observed due to strong hydrogen bonding between the water molecules, which causes molecular clustering and pore-filling [62–65]. Other than the sorption curve's shape, the water adsorption's onset is influenced by higher activation temperatures and shifts to lower RHs. This observation agrees with previous reports [59,60,62]. As observed for thermally activated samples, functional surface groups and pores cause water uptake at lower humidity. Additionally, the slope of the sorption curve is steeper at higher activation temperatures, indicating an increased sorption ability. The desorption curves of all samples, representing the reverse process of releasing water, differ from the sorption curves and display a hysteresis loop characteristic for the H2 type [64]. Such hysteresis is typically ascribed to capillary condensation in the pores and a delayed but immediate desorption of water from the pore space due to strong interactions between the water molecules [62, 64].

Overall, this section shows a significant improvement in the wettability of the carbon felts by thermal activation and the successful

quantification by DVS. It also shows that the improved wettability can be correlated to an increased amount of oxygen functional groups, which was determined in the XPS measurements. However, the type V isotherm observed even at high activation temperatures implies that the interaction between the water vapor and the samples is still relatively weak. Since a water droplet is already entirely absorbed by the sample activated at 400°C , the slight increase in the water sorption ability is enough to wet the carbon felt. Higher temperatures further improve the wettability, which is beneficial for electrode wetting and increases the interface between the electrode and the electrolyte. Standard analysis by contact angle measurements can give a first impression of carbon felts' wettability. However, it must be considered that carbon felts exhibit rough surfaces, and the thermally activated felts absorb a water droplet immediately, rendering a contact angle measurement impossible. Here, DVS measurements can fill the gap. They provide quantitative information on the water sorption capacity and can be used to compare and distinguish differences in the wettability, e.g., from samples activated at different temperatures. Furthermore, the type of sorption isotherms provides additional information on the water sorption behavior, indicating the extent of wettability changes.

3.3. Electrochemical performance

Previous publications agree that thermal activation procedures for porous carbon-based electrodes considerably improve the cell performance of VRFBs [17–21,24–26]. However, contradictory trends in wettability and sample stability make it difficult to find the optimum activation temperature for carbon felt electrodes. Electrochemical measurements were performed in vanadium(IV) electrolyte to further study the impact of the temperature on the performance of the herein-presented electrodes in the positive half-cell of a VRFB. The focus was put on this half cell to present a thorough analysis via CV and EIS combined with DRT analysis.

Fig. 7 (a) and (b) display CV measurements of the different samples in the potential range of the vanadium(IV)/vanadium(V) redox reaction. Only, the measurements at 2 mVs^{-1} are presented herein. However, no significant variations were observed at other scan rates, as shown in the Supporting Information (Figure S. 7). For clarity, the CV measurements are separated into two graphs showing different ranges of applied activation temperatures. Fig. 7 (c) summarizes the correlation between the activation temperature and different electrochemical parameters, such as the anodic and the cathodic peak potential (E_{pa} and E_{pc}), the halfway potential ($E_{1/2}$), and the peak-to-peak separation (ΔE).

Fig. 7 (a) shows that the electrochemical response of the carbon felt stays very similar to the pristine sample up to an activation temperature of 300°C . These measurements have significant peak-to-peak separations of around 0.4 V, peak current ratios of around 0.5, and the shape and size of the oxidation and the reduction peak differ strongly, implying limited reversibility of the vanadium(IV)/vanadium(V) redox reaction and the electron transfer at the electrodes. Furthermore, the full width at half maximum (FWHM) of the peaks in the backward scan is about 1.5 times wider than in the forward scan, speaking of approximately 0.3 V and 0.2 V for the pristine sample, respectively. These values show that the vanadium(IV)/vanadium(V) redox reaction is not entirely reversible for these samples and differs significantly from the ideal FWHM of a reversible one-electron redox reaction [66]. The reduction reaction is considerably slower and more sluggish. A further increase in activation temperature to 350°C and 400°C reduces the peak-to-peak separations to around 0.17 V and 0.06 V, respectively. Furthermore, the peak current ratios increase to 0.9, and the oxidation and the reduction peak have a similar shape and size in both measurements, indicating a significantly improved electron transfer and reversibility of the redox reaction. This observation is also supported by very similar FWHMs of both redox peaks. At 400°C , the FWHM of both peaks amounts to around 0.1 V. This value is substantially closer to the ideal one-electron redox reaction [66], implying a considerably

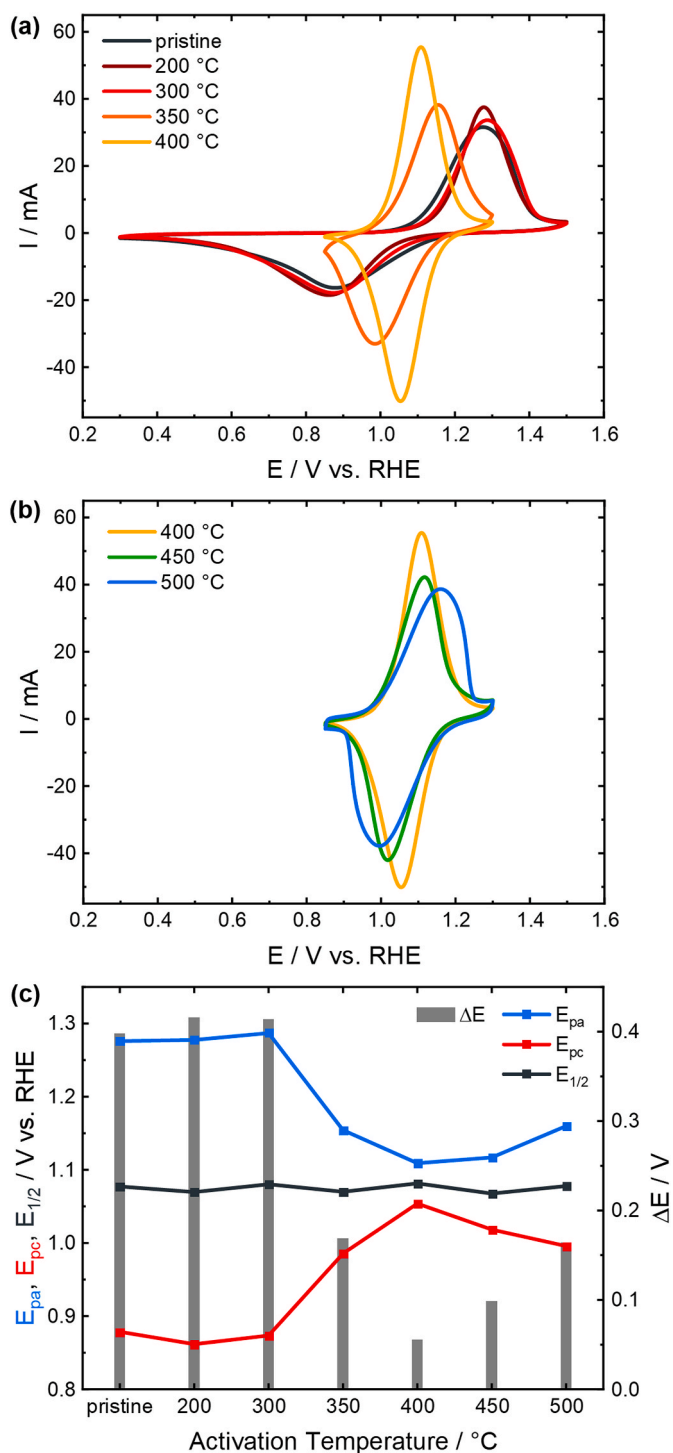


Fig. 7. (a), (b) CV measurements of pristine and activated SIGRACELL® GFA 6 EA carbon felts in 0.1 M VOSO_4 in 2.0 M H_2SO_4 at a scan rate of 2 mVs^{-1} . (c) Electrochemical analysis of the cyclic voltammograms displaying the correlation between the activation temperature and the anodic and the cathodic peak potential (E_{pa} and E_{pc}), the halfway potential ($E_{1/2}$), and the peak-to-peak separation (ΔE).

improved reaction reversibility, mainly due to the improved reduction reaction. We assume that the changes in surface functional groups and graphitic structure, determined by XPS measurements, enhance the activity of the reduction reaction in particular [67]. Thereby, the reversibility of the redox couple improves significantly. Furthermore, the peak currents increase with higher activation temperature, implying an

improved electrode performance. The similarities in the shape, size, FWHM, and current maximum of both redox peaks prevail for higher activation temperatures of 450 °C and 500 °C, but the width of the peak gets broader, the peak currents decrease slightly, and the peak-to-peak separation increases to around 0.10 V and 0.16 V, respectively. In addition, an increased double-layer capacity can be observed at higher treatment temperatures. We assume that these observations can be attributed to the harsher oxidation environment at higher temperatures, which causes carbon decomposition, significant structural changes, and the loss of preferable reaction sites. In a recent study, Lindner et al. [22] investigated the effect of thermal treatment duration on the electrochemical activity of PAN-based carbon felts. In agreement with the herein-reported results, they found an initial improvement in electrochemical activity correlated to the treatment duration, followed by a decline for longer treatments. This study observes a similar switch in the electrochemical performance at 400 °C. In addition to the peak-to-peak separation, the halfway potential is another essential electrochemical parameter since it corresponds to the standard potential E^0 of the redox active species at standard conditions [66]. In this series of measurements, the active redox species stays the same; therefore, the halfway potential should be constant. The electrochemical analysis in Fig. 7 (c) supports this statement since the halfway potential stays consistent at around 1.1 V vs. RHE, which is in good agreement with the reported standard potential of 0.991 V vs. RHE for the vanadium(IV)/vanadium (V) redox reaction [68].

In summary, this measurement series shows that the carbon felt activated at 400 °C exhibits the most promising electrochemical performance in the vanadium(IV)/vanadium(V) redox reaction. The lowest peak-to-peak separation is observed at this electrode, and both peaks look almost identical in shape and size, indicating good reversibility of the redox reaction and a similar electron transfer for the reduction and oxidation reaction. At lower and higher activation temperatures, the electrochemical activity and the reversibility are worse, indicating 400 °C as the optimum in these measurements.

Additionally, EIS data were recorded and further analyzed using the DRT method to separate the individual processes. Thereby, no specific equivalent circuit but an infinite number of RC-elements connected in series with an ohmic resistance is used to fit the EIS data [29,69]. This approach is relatively new in the field of VRFBs and has only been used by Schneider et al. [70] for full-cell studies and by Schilling et al. [28] to investigate the vanadium(IV)/vanadium(V) half-cell reaction. For the first time, we show how DRT analysis can provide insight into the contributions of treated carbon electrodes to the total impedance and how thermal activation influences the individual processes of the vanadium(IV)/vanadium(V) reaction. In this study, three distinguished features are usually present in the DRT spectrum: one peak in the low-frequency range ($< 25 \text{ mHz}$), several peaks in the medium-frequency range (25 mHz – 100 Hz), and one peak in the high-frequency range ($> 100 \text{ Hz}$). Schilling et al. [28] identified these ranges as the ion transport, the transport through the porous electrode, and the electrochemical reaction, respectively. Fig. 8 summarizes the results of the DRT analysis. Fig. 8 (a) and (b) display the same data in two charts highlighting different aspects. The EIS data and the corresponding DRT spectra can be found in the Supporting Information (Figure S. 8).

The bar chart in Fig. 8 (a) shows a similar total impedance for the pristine sample (44.3 Ω), and the sample activated at 300 °C (32.9 Ω). This result supports the previous observations from the CV measurements since the electrochemical response of the pristine sample and the sample activated at 300 °C are nearly identical. Fig. 8 (b) displays how the impedances of the individual processes contribute to the total impedance. For these electrochemically inactive samples, the impedance in the medium-frequency range contributes more than 80%, severely limiting the performance. This frequency range is ascribed to the transport through the porous structure of the electrode, which is affected by the electrode structure, the wettability, and the surface

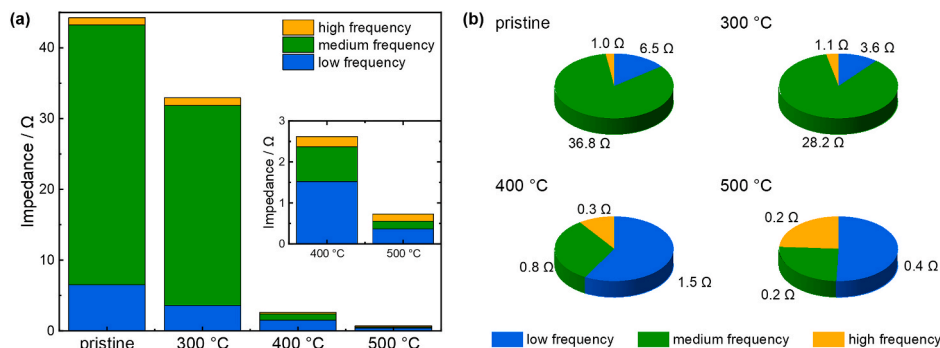


Fig. 8. Results from the DRT analysis of EIS measurements of pristine and activated SIGRACELL® GFA 6 EA carbon felts summarized in (a) a bar chart (inset: zoomed in on 400 °C and 500 °C data) and (b) a pie chart for greater clarity. Both charts show the same data in two different display options. The measurements were conducted in 0.1 M VOSO₄ in 2.0 M H₂SO₄ at a potential of 1.05 V vs. RHE at a flow rate of 15 mLmin⁻¹.

composition. In this case, the electrode structure of both samples was determined by SEM to be very similar, and the hindered transport might primarily be caused by the felts' low wettability and lower amount of oxygen functional groups, as discussed in section 3.2. Since the aqueous electrolyte is pumped through the electrode to reach the reaction sites, a low wettability hampers the transport and causes a significant contribution to the impedance. In comparison, a significant drop in total impedance is observed for the samples after activation at 400 °C (2.6 Ω) and 500 °C (0.8 Ω), which agrees with the report from Greco et al. [20]. The impedance decline is mainly due to the reduced transport resistance through the porous electrode, although decreased impedances are observed over the entire frequency range. At and above 400 °C, the ion transport resistance accounts for over 50% of the total impedance. The slight improvement in wettability observed for the 400 °C sample in section 3.2, already significantly facilitates the electrode transport process. The formation of pores further reduces the electrode transport impedance due to increased active surface area. Furthermore, the impedance of the ion transport also decreases with higher activation temperature due to the higher electrode wettability and surface area, improving the transport of the vanadium species to the reaction sites. The peak at the highest frequency is ascribed to the electrochemical reaction. It remains similar for the pristine and the 300 °C samples but diminishes and shifts to higher frequencies at higher activation temperatures. This observation can be explained by a faster and facilitated electrochemical reaction, which agrees with the previous CV measurements.

In summary, these EIS measurements prove that activating the carbon felt electrodes at or above 400 °C significantly decreases the total impedance in the positive half-cell of VRFBs. DRT analysis revealed the medium-frequency processes linked to the transport process through the electrode and thereby probed the electrode's wettability. The impedance of these processes is significantly reduced by thermal activation, which fits the measured increase in electrode wettability caused by a higher oxygen content in the carbon felt. The lowest impedances are observed at the highest activation temperature, corresponding to the most hydrophilic electrode. The analysis of EIS data via DRT is very convenient. Compared to the standard analysis using fits with equivalent electrical circuits, this method can be used without prior profound knowledge about the measured system. Thereby, the received DRT spectrum shows several peaks corresponding to the number of observed processes. Further, it contains the frequency information, and the impedance of the individual processes can be obtained by integrating the respective peak area. These points render DRT analysis valuable for separating the cell processes to compare different materials.

4. Conclusions

Thermal treatment is a standard procedure to improve the

performance of carbon electrodes for VRFBs. However, the complex mechanisms behind this procedure are not yet fully understood, and the effects on electrode properties are difficult to decouple. This work studied the impact of thermal activation and activation temperature on rayon-based carbon felts in a multimodal characterization approach combining standard techniques with techniques not yet established in this research area. For the first time, AFM and DVS measurements were conducted in the context of VRFB electrodes to focus on the changes in structure and wettability and how these impact the electrochemical performance. Furthermore, DRT analysis of EIS measurements was used to study the influence of electrode changes from thermal activation on the individual processes of the vanadium(IV)/vanadium(V) reaction. Line scan analysis of AFM images provided major insights into the structure and morphology of the samples and quantitative information on the size and depth of strings and pores. We observed pore formation mainly in the nanometer range and increased roughness for samples activated above 300 °C but increased fragility and mass loss for activation temperatures at or above 450 °C. DVS measurements showed that the water sorption ability of the carbon felts improved with thermal activation since the water uptake at 90% RH increased from 0.0 wt% for the pristine sample to 11.7 wt% at 500 °C. Still, the observed type V sorption isotherm indicates a relatively hydrophobic nature of the samples and weak interaction between the samples and the water adsorbate. Both, the sample degradation and the improved wettability, could be correlated to the results from XPS measurements, which showed an increased oxygen content and a lower amount of carbon at higher activation temperatures. Additional CV measurements showed a significant improvement in redox reversibility after thermal activation, and a minimum peak-to-peak separation of around 0.06 V for the sample activated at 400 °C. Further, EIS measurements coupled with DRT analysis revealed a significant drop in total impedance from 44.3 Ω for the pristine sample to 0.8 Ω for the 500 °C sample. Additionally, the transport through the electrode, corresponding to the impedance in the medium-frequency range, contributes a major share to the total impedance of the pristine and the 300 °C samples and diminishes considerably at higher activation temperatures. Correlating this observation to the increased wettability of the samples observed during the DVS measurements shows that the DRT analysis can give electrochemical insights and indicate changes in the wettability of electrode materials. Overall, we conclude that the rayon-based carbon felt of this study is preferably activated for 25 h at 400 °C. This temperature is a threshold for structural changes, fiber integrity, wettability, and electrochemical performance. Higher temperatures improve the wettability but strongly reduce the stability of the carbon fibers, cause carbon decomposition, and impair the electrochemical activity. Analogous studies on the influence of treatment duration can be of great interest to find the optimum treatment conditions. Finally, we could show that the novel approach of studying VRFB electrodes with AFM, DVS, and DRT

analysis was successful. The unique combination of non-standard techniques provides valuable new insights and complementary information on structure and wettability – beneficial for characterizing other types of electrodes.

CRedit authorship contribution statement

K. Köble: Methodology, Formal analysis, Investigation, Data curation, Writing – original draft. **M. Jaugstetter:** Formal analysis, Investigation, Data curation, Visualization, Writing – review & editing. **M. Schilling:** Formal analysis, Investigation, Data curation, Writing – review & editing. **M. Braig:** Formal analysis, Data curation, Writing – review & editing. **T. Diemant:** Formal analysis, Investigation, Data curation, Writing – review & editing. **K. Tschulik:** Supervision, Project administration, Funding acquisition, Writing – review & editing. **R. Zeis:** Conceptualization, Methodology, Supervision, Project administration, Funding acquisition, Writing – review & editing.

Declaration of competing interest

The authors declare that they have no known competing financial interests or personal relationships that could have appeared to influence the work reported in this paper.

Data availability

Data will be made available on request.

Acknowledgments

We thank Vanessa Scherer for her help in preparing and measuring the AFM samples. We gratefully acknowledge SGL Carbon for the supply of SIGRACELL® carbon felts. K. K. and M. S. gratefully acknowledge financial support through a Kekulé Ph.D. fellowship by the Fonds der Chemischen Industrie (FCI). This work contributes to the research performed at CELEST (Center for Electrochemical Energy Storage Ulm-Karlsruhe). M. J. thanks the Research Training group "Confinement controlled Chemistry", funded by the Deutsche Forschungsgemeinschaft (DFG, German Research Foundation)-GRK2376/331085229. This "Center for Solvation Science ZEMOS" supported this work, funded by the German Federal Ministry of Education and Research (BMBF) and the Ministry of Culture and Research of Nord Rhine-Westphalia.

Appendix A. Supplementary data

Supplementary data to this article can be found online at <https://doi.org/10.1016/j.jpowsour.2023.233010>.

References

- M. Skyllas-Kazacos, M.H. Chakrabarti, S.A. Hajimolana, F.S. Mjalli, M. Saleem, Progress in flow battery research and development, *J. Electrochem. Soc.* 158 (2011) R55, <https://doi.org/10.1149/1.3599565>.
- B. Dunn, H. Kamath, J.-M. Tarascon, Electrical energy storage for the grid: a battery of choices, *Science* 334 (2011) 928–935, <https://doi.org/10.1126/science.1212741>, 80.
- A.Z. Weber, M.M. Mench, J.P. Meyers, P.N. Ross, J.T. Gostick, Q. Liu, Redox flow batteries: a review, *J. Appl. Electrochem.* 41 (2011) 1137–1164, <https://doi.org/10.1007/s10800-011-0348-2>.
- K. Lourenssen, J. Williams, F. Ahmadpour, R. Clemmer, S. Tasnim, Vanadium redox flow batteries: a comprehensive review, *J. Energy Storage* 25 (2019), 100844, <https://doi.org/10.1016/j.est.2019.100844>.
- P. Alotto, M. Guarnieri, F. Moro, Redox flow batteries for the storage of renewable energy: a review, *Renew. Sustain. Energy Rev.* 29 (2014) 325–335, <https://doi.org/10.1016/j.rser.2013.08.001>.
- T.X. Huang, M. Bechelany, M. Cretin, Carbon felt based-electrodes for energy and environmental applications: a review, *Carbon N. Y.* 122 (2017) 564–591, <https://doi.org/10.1016/j.carbon.2017.06.078>.
- M.H. Chakrabarti, N.P. Brandon, S.A. Hajimolana, F. Tariq, V. Yufit, M.A. Hashim, M.A. Hussain, C.T.J. Low, P.V. Aravind, Application of carbon materials in redox flow batteries, *J. Power Sources* 253 (2014) 150–166, <https://doi.org/10.1016/j.jpowsour.2013.12.038>.
- J. Melke, P. Jakes, J. Langner, L. Riekehr, U. Kunz, Z. Zhao-Karger, A. Nefedov, H. Sezen, C. Wöll, H. Ehrenberg, C. Roth, Carbon materials for the positive electrode in all-vanadium redox flow batteries, *Carbon N. Y.* 78 (2014) 220–230, <https://doi.org/10.1016/j.carbon.2014.06.075>.
- J. Melke, J. Martin, M. Bruns, P. Hügenell, A. Schökel, S. Montoya Isaza, F. Fink, P. Elsässer, A. Fischer, Investigating the effect of microstructure and surface functionalization of mesoporous N-doped carbons on V 4+/V 5+ kinetics, *ACS Appl. Energy Mater.* 3 (2020) 11627–11640, <https://doi.org/10.1021/acsaem.0c01489>.
- J.H. Vinco, A.E.E.C. Domingos, D.C.R. Espinosa, J.A.S. Tenório, M.P.G. Baltazar, Unfolding the Vanadium Redox Flow Batteries: an in-depth perspective on its components and current operation challenges, *J. Energy Storage* 43 (2021), 103180, <https://doi.org/10.1016/j.est.2021.103180>.
- L. Eifert, Z. Jusys, R.J. Behm, R. Zeis, Side reactions and stability of pre-treated carbon felt electrodes for vanadium redox flow batteries: a DEMS study, *Carbon N. Y.* 158 (2020) 580–587, <https://doi.org/10.1016/j.carbon.2019.11.029>.
- L. Eifert, Z. Jusys, R. Banerjee, R.J. Behm, R. Zeis, Differential electrochemical mass spectrometry of carbon felt electrodes for vanadium redox flow batteries, *ACS Appl. Energy Mater.* 1 (2018) 6714–6718, <https://doi.org/10.1021/acsaem.8b01550>.
- R. Schweiss, A. Pritzl, C. Meiser, Parasitic hydrogen evolution at different carbon fiber electrodes in vanadium redox flow batteries, *J. Electrochem. Soc.* 163 (2016) A2089–A2094, <https://doi.org/10.1149/2.1281609jes>.
- M. Skyllas-Kazacos, M. Rychcik, R.G. Robins, A.G. Fane, M.A. Green, New all-vanadium redox flow cell, *J. Electrochem. Soc.* 133 (1986) 1057–1058, <https://doi.org/10.1149/1.2108706>.
- N. Bevilacqua, L. Eifert, R. Banerjee, K. Köble, T. Faragó, M. Zuber, A. Bazylak, R. Zeis, Visualization of electrolyte flow in vanadium redox flow batteries using synchrotron X-ray radiography and tomography – impact of electrolyte species and electrode compression, *J. Power Sources* 439 (2019), 227071, <https://doi.org/10.1016/j.jpowsour.2019.227071>.
- L. Eifert, R. Banerjee, Z. Jusys, R. Zeis, Characterization of carbon felt electrodes for vanadium redox flow batteries: impact of treatment methods, *J. Electrochem. Soc.* 165 (2018) A2577–A2586, <https://doi.org/10.1149/2.0531811jes>.
- S. Zhong, C. Padeste, M. Kazacos, M. Skyllas-Kazacos, Comparison of the physical, chemical and electrochemical properties of rayon- and polyacrylonitrile-based graphite felt electrodes, *J. Power Sources* 45 (1993) 29–41, [https://doi.org/10.1016/0378-7753\(93\)80006-B](https://doi.org/10.1016/0378-7753(93)80006-B).
- B. Sun, M. Skyllas-Kazacos, Modification of graphite electrode materials for vanadium redox flow battery application—I. Thermal treatment, *Electrochim. Acta* 37 (1992) 1253–1260, [https://doi.org/10.1016/0013-4686\(92\)85064-R](https://doi.org/10.1016/0013-4686(92)85064-R).
- A.M. Pezeshki, J.T. Clement, G.M. Veith, T.A. Zawodzinski, M.M. Mench, High performance electrodes in vanadium redox flow batteries through oxygen-enriched thermal activation, *J. Power Sources* 294 (2015) 333–338, <https://doi.org/10.1016/j.jpowsour.2015.05.118>.
- K.V. Greco, A. Forner-Cuenca, A. Mularczyk, J. Eller, F.R. Brushett, Elucidating the nuanced effects of thermal pretreatment on carbon paper electrodes for vanadium redox flow batteries, *ACS Appl. Mater. Interfaces* 10 (2018) 44430–44442, <https://doi.org/10.1021/acsami.8b15793>.
- K.V. Greco, J.K. Bonesteel, N. Chanut, C. Tai-Chieh Wan, Y.-M. Chiang, F. R. Brushett, Limited accessibility to surface area generated by thermal pretreatment of electrodes reduces its impact on redox flow battery performance, *ACS Appl. Energy Mater.* 4 (2021) 13516–13527, <https://doi.org/10.1021/acsaem.1c01980>.
- A. Lindner, H. Radinger, F. Scheiba, H. Ehrenberg, Structure–activity correlation of thermally activated graphite electrodes for vanadium flow batteries, *RSC Adv.* 12 (2022) 14119–14126, <https://doi.org/10.1039/D2RA02368G>.
- P.C. Ghimire, R. Schweiss, G.G. Scherer, T.M. Lim, N. Wai, A. Bhattarai, Q. Yan, Optimization of thermal oxidation of electrodes for the performance enhancement in all-vanadium redox flow batteries, *Carbon N. Y.* 155 (2019) 176–185, <https://doi.org/10.1016/j.carbon.2019.08.068>.
- D. Dixon, D.J. Babu, J. Langner, M. Bruns, L. Pfaffmann, A. Bhaskar, J.J. Schneider, F. Scheiba, H. Ehrenberg, Effect of oxygen plasma treatment on the electrochemical performance of the rayon and polyacrylonitrile based carbon felt for the vanadium redox flow battery application, *J. Power Sources* 332 (2016) 240–248, <https://doi.org/10.1016/j.jpowsour.2016.09.070>.
- J. Langner, M. Bruns, D. Dixon, A. Nefedov, C. Wöll, F. Scheiba, H. Ehrenberg, C. Roth, J. Melke, Surface properties and graphitization of polyacrylonitrile based fiber electrodes affecting the negative half-cell reaction in vanadium redox flow batteries, *J. Power Sources* 321 (2016) 210–218, <https://doi.org/10.1016/j.jpowsour.2016.04.128>.
- D. Kil, H.J. Lee, S. Park, S. Kim, H. Kim, Synthesis of activated graphite felts using short-term ozone/heat treatment for vanadium redox flow batteries, *J. Electrochem. Soc.* 164 (2017) A3011–A3017, <https://doi.org/10.1149/2.0311713jes>.
- Q. Wu, X. Zhang, Y. Lv, L. Lin, Y. Liu, X. Zhou, Bio-inspired multiscale-pore-network structured carbon felt with enhanced mass transfer and activity for vanadium redox flow batteries, *J. Mater. Chem. A.* 6 (2018) 20347–20355, <https://doi.org/10.1039/C8TA06445H>.
- M. Schilling, M. Braig, K. Köble, R. Zeis, Investigating the V(IV)/V(V) electrode reaction in a vanadium redox flow battery – a distribution of relaxation times analysis, *Electrochim. Acta* 430 (2022), 141058, <https://doi.org/10.1016/j.electacta.2022.141058>.

- [29] T.H. Wan, M. Saccoccio, C. Chen, F. Ciucci, Influence of the discretization methods on the distribution of relaxation times deconvolution: implementing radial basis functions with DRTools, *Electrochim. Acta* 184 (2015) 483–499, <https://doi.org/10.1016/j.electacta.2015.09.097>.
- [30] T.J. Rabbow, M. Trampert, P. Pokorny, P. Binder, A.H. Whitehead, Variability within a single type of polyacrylonitrile-based graphite felt after thermal treatment. Part II: chemical properties, *Electrochim. Acta* 173 (2015) 24–30, <https://doi.org/10.1016/j.electacta.2015.05.058>.
- [31] T.J. Rabbow, M. Trampert, P. Pokorny, P. Binder, A.H. Whitehead, Variability within a single type of polyacrylonitrile-based graphite felt after thermal treatment. Part I: physical properties, *Electrochim. Acta* 173 (2015) 17–23, <https://doi.org/10.1016/j.electacta.2015.05.020>.
- [32] J.-H. Kim, S. Ryu, S. Maurya, J.-Y. Lee, K.-W. Sung, J.-S. Lee, S.-H. Moon, Fabrication of a composite anion exchange membrane with aligned ion channels for a high-performance non-aqueous vanadium redox flow battery, *RSC Adv.* 10 (2020) 5010–5025, <https://doi.org/10.1039/C9RA08616A>.
- [33] X. Teng, J. Dai, J. Su, Y. Zhu, H. Liu, Z. Song, A high performance polytetrafluoroethene/Nafion composite membrane for vanadium redox flow battery application, *J. Power Sources* 240 (2013) 131–139, <https://doi.org/10.1016/j.jpowsour.2013.03.177>.
- [34] C. Jia, Y. Cheng, X. Ling, G. Wei, J. Liu, C. Yan, Sulfonated poly(Ether Ether ketone)/functionalized carbon nanotube composite membrane for vanadium redox flow battery applications, *Electrochim. Acta* 153 (2015) 44–48, <https://doi.org/10.1016/j.electacta.2014.11.123>.
- [35] T.S. Watkins, D. Sarbapalli, M.J. Counihan, A.S. Danis, J. Zhang, L. Zhang, K. R. Zavadil, J. Rodríguez-López, A combined SECM and electrochemical AFM approach to probe interfacial processes affecting molecular reactivity at redox flow battery electrodes, *J. Mater. Chem. A* 8 (2020) 15734–15745, <https://doi.org/10.1039/D0TA00836B>.
- [36] H. Gursu, M. Gençten, Y. Şahin, Synthesis of phosphorus doped graphenes via the yucl's method as the positive electrode of a vanadium redox flow battery, *J. Electrochem. Soc.* 168 (2021), 060504, <https://doi.org/10.1149/1945-7111/ac0457>.
- [37] H. Gürsu, M. Gençten, Y. Şahin, Preparation of N-doped graphene-based electrode via electrochemical method and its application in vanadium redox flow battery, *Int. J. Energy Res.* 42 (2018) 3851–3860, <https://doi.org/10.1002/er.4117>.
- [38] H. Liu, Q. Xu, C. Yan, Y. Qiao, Corrosion behavior of a positive graphite electrode in vanadium redox flow battery, *Electrochim. Acta* 56 (2011) 8783–8790, <https://doi.org/10.1016/j.electacta.2011.07.083>.
- [39] P.V. Ravi, D.T. Thangadurai, K. Nehru, Y.I. Lee, D. Nataraj, S. Thomas, N. Kalarikkal, J. Jose, Surface and morphology analyses, and voltammetry studies for electrochemical determination of cerium(III) using a graphene nanobud-modified-carbon felt electrode in acidic buffer solution (pH 4.0 ± 0.05), *RSC Adv.* 10 (2020) 37409–37418, <https://doi.org/10.1039/D0RA07555H>.
- [40] L.B. Nohara, G. Petracconi Filho, E.L. Nohara, M.U. Kleinke, M.C. Rezende, Evaluation of carbon fiber surface treated by chemical and cold plasma processes, *Mater. Res.* 8 (2005) 281–286, <https://doi.org/10.1590/S1516-14392005000300010>.
- [41] J.-S. Lee, T.-J. Kang, Changes in physico-chemical and morphological properties of carbon fiber by surface treatment, *Carbon N. Y.* 35 (1997) 209–216, [https://doi.org/10.1016/S0008-6223\(96\)00138-8](https://doi.org/10.1016/S0008-6223(96)00138-8).
- [42] W.P. Hoffman, Scanning probe microscopy of carbon fiber surfaces, *Carbon N. Y.* 30 (1992) 315–331, [https://doi.org/10.1016/0008-6223\(92\)90026-S](https://doi.org/10.1016/0008-6223(92)90026-S).
- [43] C. Brasquet, B. Rousseau, H. Estrade-Szwarcopf, P. Le Cloirec, Observation of activated carbon fibres with SEM and AFM correlation with adsorption data in aqueous solution, *Carbon N. Y.* 38 (2000) 407–422, [https://doi.org/10.1016/S0008-6223\(99\)00120-7](https://doi.org/10.1016/S0008-6223(99)00120-7).
- [44] G.X. Wang, H. Han, L.W. Li, H.Y. Quan, Y.P. Shi, W.Z. Qin, P. Lu, Q.L. Wu, SEM and AFM studies on the surface and cross section morphology of rayon-based activated carbon fibers, *Mater. Sci. Forum* 689 (2011) 413–418, <https://doi.org/10.4028/www.scientific.net/MSF.689.413>.
- [45] M.V. Evers, M. Bernal, B. Roldan Cuenya, K. Tschulik, Piece by piece—electrochemical synthesis of individual nanoparticles and their performance in ORR electrocatalysis, *Angew. Chem. Int. Ed.* 58 (2019) 8221–8225, <https://doi.org/10.1002/anie.201813993>.
- [46] H.P. Boehm, Chemical Identification of Surface Groups, *Adv. Catal.*, 1966, pp. 179–274, [https://doi.org/10.1016/S0360-0564\(08\)60354-5](https://doi.org/10.1016/S0360-0564(08)60354-5).
- [47] R. Banerjee, N. Bevilacqua, L. Eifert, R. Zeis, Characterization of carbon felt electrodes for vanadium redox flow batteries – a pore network modeling approach, *J. Energy Storage* 21 (2019) 163–171, <https://doi.org/10.1016/j.est.2018.11.014>.
- [48] F. Tariq, J. Rubio-García, V. Yufit, A. Bertei, B.K. Chakrabarti, A. Kucernak, N. Brandon, Uncovering the mechanisms of electrolyte permeation in porous electrodes for redox flow batteries through real time in situ 3D imaging, *Sustain. Energy Fuels* 2 (2018) 2068, <https://doi.org/10.1039/C8SE00174J>. –2080.
- [49] M. Gebhard, M. Schnucklake, A. Hilger, M. Röhe, M. Osenberg, U. Krewer, I. Manke, C. Roth, X-Ray-Computed radiography and tomography study of electrolyte invasion and distribution inside pristine and heat-treated carbon felts for redox flow batteries, *Energy Technol.* 8 (2020), 1901214, <https://doi.org/10.1002/ente.201901214>.
- [50] K. Köble, L. Eifert, N. Bevilacqua, K.F. Fahy, A. Bazylak, R. Zeis, Synchrotron X-Ray radiography of vanadium redox flow batteries – time and spatial resolved electrolyte flow in porous carbon electrodes, *J. Power Sources* 492 (2021), 229660, <https://doi.org/10.1016/j.jpowsour.2021.229660>.
- [51] L. Eifert, N. Bevilacqua, K. Köble, K. Fahy, L. Xiao, M. Li, K. Duan, A. Bazylak, P. Sui, R. Zeis, Synchrotron X-ray radiography and tomography of vanadium redox flow batteries—cell design, electrolyte flow geometry, and gas bubble formation, *ChemSusChem* 13 (2020) 3154–3165, <https://doi.org/10.1002/cssc.202000541>.
- [52] R. Banerjee, N. Bevilacqua, A. Mohseninia, B. Wiedemann, F. Wilhelm, J. Scholta, R. Zeis, Carbon felt electrodes for redox flow battery: impact of compression on transport properties, *J. Energy Storage* 26 (2019), 100997, <https://doi.org/10.1016/j.est.2019.100997>.
- [53] R. Tan, A. Wang, R. Malpass-Evans, R. Williams, E.W. Zhao, T. Liu, C. Ye, X. Zhou, B.P. Darwich, Z. Fan, L. Turciani, E. Jackson, L. Chen, S.Y. Chong, T. Li, K.E. Jelfs, A.I. Cooper, N.P. Brandon, C.P. Grey, N.B. McKeown, Q. Song, Hydrophilic microporous membranes for selective ion separation and flow-battery energy storage, *Nat. Mater.* 19 (2020) 195–202, <https://doi.org/10.1038/s41563-019-0536-8>.
- [54] C. Ye, A. Wang, C. Breakwell, R. Tan, C. Grazia Bezzu, E. Hunter-Sellers, D. R. Williams, N.P. Brandon, P.A.A. Klusener, A.R. Kucernak, K.E. Jelfs, N. B. McKeown, Q. Song, Development of efficient aqueous organic redox flow batteries using ion-sieving sulfonated polymer membranes, *Nat. Commun.* 13 (2022) 3184, <https://doi.org/10.1038/s41467-022-30943-y>.
- [55] J. Yuan, Q. Chen, B. Fei, Investigation of the water vapor sorption behavior of bamboo fibers with different sizes, *Eur. J. Wood Wood Prod.* 79 (2021) 1131–1139, <https://doi.org/10.1007/s00107-020-01652-4>.
- [56] X. Guo, Y. Wu, X. Xie, Water vapor sorption properties of cellulose nanocrystals and nanofibers using dynamic vapor sorption apparatus, *Sci. Rep.* 7 (2017), 14207, <https://doi.org/10.1038/s41598-017-14664-7>.
- [57] X. Shen, D. Guo, P. Jiang, S. Yang, G. Li, F. Chu, Water vapor sorption mechanism of furfurylated wood, *J. Mater. Sci.* 56 (2021) 11324–11334, <https://doi.org/10.1007/s10853-021-06041-7>.
- [58] X. Zhang, J. Li, Y. Yu, H. Wang, Investigating the water vapor sorption behavior of bamboo with two sorption models, *J. Mater. Sci.* 53 (2018) 8241–8249, <https://doi.org/10.1007/s10853-018-2166-y>.
- [59] J. Alcañiz-Monge, A. Linares-Solano, B. Rand, Water adsorption on activated carbons: study of water adsorption in micro- and mesopores, *J. Phys. Chem. B* 105 (2001) 7998–8006, <https://doi.org/10.1021/jp010674b>.
- [60] J. Alcañiz-Monge, A. Linares-Solano, B. Rand, Mechanism of adsorption of water in carbon micropores as revealed by a study of activated carbon fibers, *J. Phys. Chem. B* 106 (2002) 3209–3216, <https://doi.org/10.1021/jp014388b>.
- [61] M.M. Dubinin, Water vapor adsorption and the microporous structures of carbonaceous adsorbents, *Carbon N. Y.* 18 (1980) 355–364, [https://doi.org/10.1016/0008-6223\(80\)90007-X](https://doi.org/10.1016/0008-6223(80)90007-X).
- [62] L. Liu, S. Johnathan Tan, T. Horikawa, D.D. Do, D. Nicholson, J. Liu, Water adsorption on carbon - a review, *Adv. Colloid Interface Sci.* 250 (2017) 64–78, <https://doi.org/10.1016/j.cis.2017.10.002>.
- [63] T. Soboleva, K. Malek, Z. Xie, T. Navessin, S. Holdcroft, PEMFC catalyst layers: the role of micropores and mesopores on water sorption and fuel cell activity, *ACS Appl. Mater. Interfaces* 3 (2011) 1827–1837, <https://doi.org/10.1021/am200590w>.
- [64] M. Thommes, K. Kaneko, A.V. Neimark, J.P. Olivier, F. Rodriguez-Reinoso, J. Rouquerol, K.S.W. Sing, Physisorption of gases, with special reference to the evaluation of surface area and pore size distribution (IUPAC Technical Report), *Pure Appl. Chem.* 87 (2015) 1051–1069, <https://doi.org/10.1515/pac-2014-1117>.
- [65] J.J. Mahle, An adsorption equilibrium model for Type 5 isotherms, *Carbon N. Y.* 40 (2002) 2753–2759, [https://doi.org/10.1016/S0008-6223\(02\)00201-4](https://doi.org/10.1016/S0008-6223(02)00201-4).
- [66] N. Elgrishi, K.J. Rountree, B.D. McCarthy, E.S. Rountree, T.T. Eisenhart, J. L. Dempsey, A practical beginner's guide to cyclic voltammetry, *J. Chem. Educ.* 95 (2018) 197–206, <https://doi.org/10.1021/acs.jchemed.7b00361>.
- [67] M. Steimecke, S. Rümmler, N.-F. Schuhmacher, T. Lindenberger, M. Hartmann, M. Bron, A comparative study of functionalized high-purity carbon nanotubes towards the V(IV)/V(V) redox reaction using cyclic voltammetry and scanning electrochemical microscopy, *Electroanalysis* 29 (2017) 1056–1061, <https://doi.org/10.1002/elan.201600614>.
- [68] W.M. Haynes, D.R. Lide, T.J. Bruno (Eds.), *CRC Handbook of Chemistry and Physics*, 97th ed., CRC Press, 2016 <https://doi.org/10.1201/9781315380476>.
- [69] M.A. Danzer, Generalized distribution of relaxation times analysis for the characterization of impedance spectra, *Batteries* 5 (2019) 53, <https://doi.org/10.3390/batteries5030053>.
- [70] J. Schneider, T. Tichter, P. Khadke, R. Zeis, C. Roth, Deconvolution of electrochemical impedance data for the monitoring of electrode degradation in VRFB, *Electrochim. Acta* 336 (2020), 135510, <https://doi.org/10.1016/j.electacta.2019.135510>.